International Journal of Innovative Research and Scientific Studies, 8(9) 2025, pages: 292-299

ISSN: 2617-6548

URL: www.ijirss.com

A study on freezing technology for the safe storage and transportation of spent lithium-ion batteries

Yong-Ho Yeo[1], Jei-Pil Wang[2*]

[1,2]*Department of Metallurgical Engineering, Pukyong National University, Busan 48513, Republic of Korea.*

Corresponding author: Jei-Pil Wang (*Email: jpwang@pknu.ac.kr*)

Abstract

This study investigates cryogenic freezing as a safety measure for end-of-life (EOL) lithium-ion batteries during storage and transportation. We consider immersion and indirect heat-exchange architectures compatible with liquid nitrogen (LN_2) or liquefied air (LA), and evaluate pre-/post-freezing changes in module-level properties. Electrical diagnostics focus on early degradation indicators—charge/discharge capacity, direct-current internal resistance (DCIR), and insulation resistance—measured under matched protocols before and after freezing. Under the tested protocol (−50 °C, ≥24 h soak, controlled ramp, electrical isolation, gradual rewarming), no macroscopic mechanical damage was observed, and the module retained its electrochemical performance: discharge capacity remained essentially unchanged, DCIR showed no measurable increase, and insulation resistance stayed ≥ 500 MΩ. These results indicate that short-term low-temperature storage can be implemented without compromising subsequent electrical behavior, supporting the feasibility of cryogenic strategies as a risk-mitigation approach for EOL battery logistics. The findings provide baseline data for future module/pack-scale demonstrations, repeated freeze–thaw durability assessments, and comparative studies using LN_2- or LA-based cooling systems.

Keywords: Capacity retention, Cryogenic freezing, DC internal resistance (DCIR), End-of-life battery, Immersion vs. indirect heat exchange, Insulation resistance, Logistics safety.

DOI: 10.53894/ijirss.v8i9.10683
Funding: This work was supported by the Korea Battery Industry Association and the Korea Gas Technology Corporation Energy Laboratory.
History: Received: 14 August 2025 / **Revised:** 23 September 2025 / **Accepted:** 26 September 2025 / **Published:** 17 October 2025

Competing Interests: The authors declare that they have no competing interests.
Authors' Contributions: All authors contributed equally to the conception and design of the study. All authors have read and agreed to the published version of the manuscript.
Transparency: The authors confirm that the manuscript is an honest, accurate, and transparent account of the study; that no vital features of the study have been omitted; and that any discrepancies from the study as planned have been explained. This study followed all ethical practices during writing.
Publisher: Innovative Research Publishing

1. Introduction

Global efforts to mitigate climate change and environmental pollution have accelerated policies for carbon neutrality and green growth, driving rapid adoption of electric vehicles (EVs). This expansion in the EV market has led to a surge in battery demand and, consequently, to increasing challenges across the life cycle of batteries—including manufacturing, operation, end-of-life (EOL) collection, and post-use management. EOL batteries often retain substantial energy density and residual electrical charge, which introduces non-trivial hazards during storage and transportation: external insults such as impact, crushing, or short-circuiting can trigger fires or explosions [1, 2]. These safety risks hinder the development of robust systems for EOL battery collection, repurposing, and recycling, and thus constitute a critical bottleneck for a circular battery economy. At present, EOL batteries are typically handled through basic warehousing and contracted disposal logistics, with limited, systematized technologies to prevent or respond to thermal runaway, fire, or explosion during storage and transport [2]. Thermal runaway originates from self-accelerating electrochemical and exothermic reactions inside the cell and can be precipitated by external stimuli such as electrical shorting, mechanical abuse, or overheating [1]. While substantial research has focused on reuse/recycling workflows (e.g., disassembly, shredding, and metal recovery), comparatively little attention has been paid to preventive technologies that ensure intrinsic safety at the storage/transport stage [2]. Cryogenic freezing has recently emerged as a promising countermeasure. Under deep-cold conditions (≈ −60 °C or lower), electrolyte viscosity increases and interfacial electrochemical kinetics are markedly suppressed, reducing internal heat generation and the propensity for thermal runaway [3]. Several studies report that lithium-ion batteries frozen to cryogenic temperatures exhibit no thermal runaway—or significantly delayed onset—when subjected to nail penetration and impact tests [4-6]. Among candidate coolants, liquid nitrogen (LN_2) and liquefied air (LA) enable both immersion and indirect heat-exchange configurations that can mitigate fire/explosion hazards and may be adaptable to long-term storage and in-transit applications [7, 8]. Despite this potential, cryogenic strategies for EOL battery storage and transport remain at an early stage. Foundational data and engineering guidance are still lacking regarding coolant selection and conditions, freezing configurations, heat-transfer behavior, and the mechanistic basis of thermal-runaway suppression under cryogenic operation [9, 10]. To address these gaps, this study evaluates LN_2- and LA-based cryogenic freezing approaches for improving the safety of EOL battery storage and transportation. We (i) establish baseline thermal and electrochemical characteristics under sub-zero to cryogenic conditions, (ii) compare immersion versus indirect heat-exchange schemes, and (iii) identify operating windows that minimize thermal-runaway risk while preserving practicality for logistics deployment. The results provide design inputs for subsequent module-/pack-scale demonstrations and for the engineering of commercial storage and transport systems.

2. Materials and Methods

2.1. Materials

An end-of-life (EOL) lithium-ion battery module removed from a KONA EV (manufacturer anonymized as H) was used as the test specimen. The module, supplied by L Corp., has a 3P10S configuration—i.e., ten series-connected groups, each composed of three cells in parallel. The module's nominal specifications are: voltage 36.3 V, capacity 180 Ah, and energy 6.48 kWh; the measured mass of the single module used in this study was approximately 33 kg. Although classified as EOL, the module retained acceptable charge–discharge performance and insulation resistance, rendering it suitable for the cryogenic-freezing experiments conducted here. Table 1 summarizes the configuration and key specifications.

Table 1.
Configuration and specifications of the battery module used.

Item	**Value**	
Configuration (Module)	3	P
	10	S
Quantity	1	Pcs.
Nominal Voltage	36.3	V
Nominal Capacity	180	Ah
Nominal Energy	6.48	kWh
Weight	33	kg
Supplier	L Corp.	

2.2. Experimental Apparatus

All experiments were conducted with instrumentation selected to (i) control and monitor charge–discharge behavior, (ii) impose and maintain sub-zero and cryogenic thermal conditions, and (iii) measure insulation resistance of the end-of-life module before and after freezing. The charge–discharge tests were performed using an Arbin LBT-60V200A system (Arbin Instruments, USA), which was employed first to verify the initial state of the module and subsequently to compare its electrochemical response at ambient temperature and following cryogenic exposure. The system provides a maximum output of 60 V and 200 A and is equipped with two independent channels, allowing reproducible execution of matched charge–discharge protocols under different thermal histories (Figure 1a). Thermal conditioning was carried out in a GTPS 3TH2000EXD environmental chamber (GTPS, Korea). The chamber affords precise temperature control over −50 °C to +150 °C and accommodates the test article within an internal volume of 2000 × 1500 × 1000 mm. This setup was used to subject the module to extreme-temperature holds and transitions in order to assess degradation responses and to characterize pre- and post-freezing thermal behavior under controlled boundary conditions (Figure 1b).

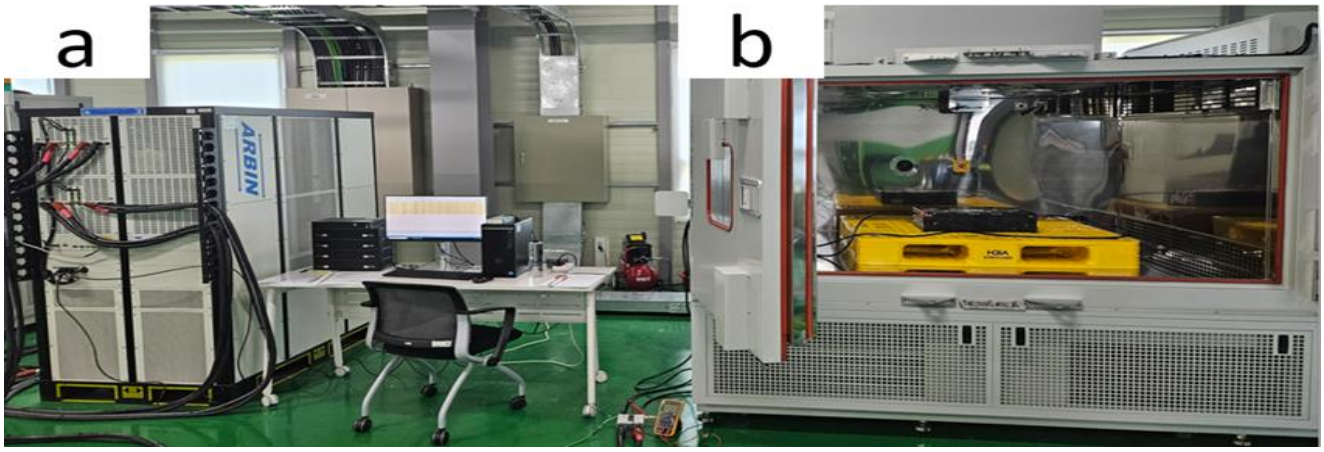

Figure 1.
Experimental equipment used in this study.
Note: (a) Arbin LBT-60V200A battery charge/discharge system; (b) GTPS 3TH2000EXD temperature–humidity chamber.

Insulation integrity was quantified using a HIOKI 3455 digital megaohmmeter (HIOKI, Japan). Measurements were pe rformed at a test voltage of 500 V, following a consistent procedure before and after cryogenic treatment to enable direct co mparison of insulation resistance. Unless otherwise specified, each measurement was repeated under identical conditions to confirm repeatability, and results were recorded immediately after the prescribed thermal exposure (Figure 2).

Figure 2.
HIOKI 3455 digital megaohmmeter used for insulation-resistance measurements.

2.3. Experimental Methods

2.3.1. Pre-Freezing Diagnostics

The test article was an EOL lithium-ion battery module recovered from an H-brand KONA EV, configured as 3P10S (nominal voltage 36.3 V; nominal capacity 180 Ah). Prior to cryogenic treatment, visual inspection and electrical characterization were performed to establish baseline values for subsequent comparison. The open-circuit voltage (OCV) was measured using an Arbin LBT-60V200A charge/discharge system, and insulation resistance was evaluated with a HIOKI 3455 digital megaohmmeter at a test voltage of 500 V DC. Following domestic industrial practice, each insulation measurement was held for 60 s; readings ≥ 500 MΩ were deemed acceptable. Before initiating the experimental sequence, inter-group voltage variation within the module was balanced to within 10 mV to ensure reliable initial conditions. These baseline measurements served as reference points for quantifying the effects of the freezing process.

2.3.2. Cryogenic Freezing Protocol

Freezing experiments were conducted in a GTPS 3TH2000EXD temperature–humidity chamber (internal volume 2000 × 1500 × 1000 mm), which accommodates large modules. Starting from ambient (~20 °C), the chamber temperature was decreased to −50 °C at a controlled ramp rate of approximately −1 °C min^{-1} to mitigate thermal-shock effects. Upon reaching the setpoint, the module was soaked for a minimum of 24 h to promote thermal equilibrium throughout the pack. This condition was selected to simulate cold-storage or cold-chain transport scenarios. During freezing, the module remained electrically isolated, and no external vibration or mechanical loading was applied.

2.3.3. Post-Freezing Diagnostics

After completion of the freezing hold, the module was removed from the chamber and allowed to warm gradually to ambient in still air; a stabilization period of ~24 h was observed prior to electrical testing. OCV and insulation resistance were then measured under the same procedures used pre-freezing to enable direct, like-for-like comparison. In addition, charge–discharge cycling was performed with the Arbin system to determine the direct-current internal resistance (DCIR)

and capacity retention. DCIR was computed from the voltage response to programmed pulse-current steps (charge and discharge assessed independently) according to DCIR=ΔV/ΔI, using the instantaneous voltage drop during the pulse. Capacity retention was evaluated at 0.5 C by repeated charge/discharge cycles and reported as the ratio of the measured discharge capacity after freezing to the initial (pre-freezing) discharge capacity. Figure 3 illustrates the post-freezing performance assessment workflow and representative measurement steps.

Figure 3.
Analysis of performance changes after freezing (Capacity, DCIR).

3. Results and Discussion

3.1. Post-Freezing Visual Inspection

A visual assessment was performed on the module before and after freezing to identify any structural damage or surface anomalies; representative post-freezing conditions of major subcomponents are shown in Figure 4. After removing the outer cover, the cell array, protection circuitry (BMS), cooling hardware, and adhesive interfaces were found to be intact. No severe deformation, swelling, or electrolyte leakage was observed on cell surfaces. The thermally conductive adhesive exhibited localized stiffening but maintained interfacial contact.

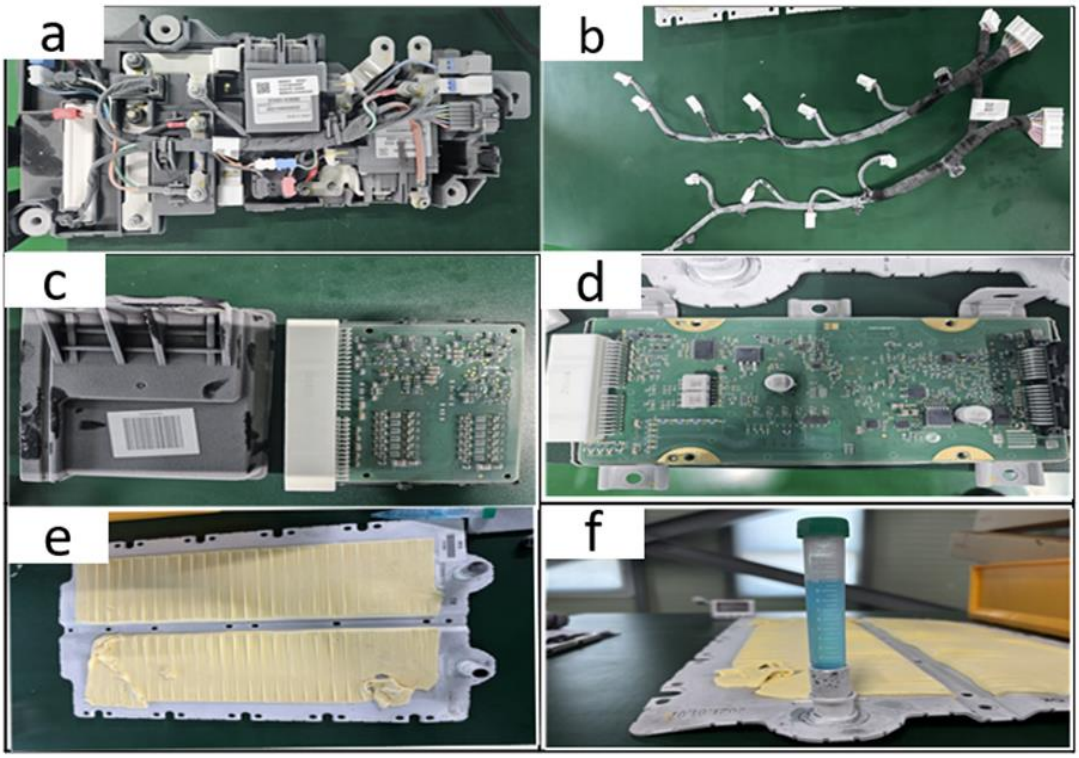

Figure 4.
Disassembled components of the end-of-life EV battery module.
Note: (a) Power Relay Assembly (PRA); (b) Cell Voltage Sensing Cables; (c) Cell Monitoring Unit (CMU); (d) Main BMS (PCB); (e) Battery Modules with Adhesive (Thermal Interface Pad); (f) Coolant-filled module during leak-tightness verification.

The adhesive—applied to ensure intimate contact between the parallel cooling sheet and the cell tops—retained its polymeric bead patterns without evident delamination. Minor spatial variations in bead thickness/coverage were noted, yielding local differences in apparent adhesion strength; such heterogeneity may influence heat-transfer uniformity and, by extensi

on, long-term cycling durability. The BMS and associated protection circuitry showed no visible mechanical damage. Both the main and slave BMS PCBs exhibited no signs of corrosion, thermal discoloration, or cracking at interconnects. Likewis e, sensing leads, busbars, and module-to-module connectors presented no evidence of wire breakage, insulation abrasion, or connector disengagement. The power relay assembly (PRA), safety plug/fuse, and harnesses retained their original position s and fixation. Importantly, no stress cracking or indications of metal fatigue were detected at busbar–connector joints—loc ations that can be susceptible to thermo-mechanical mismatch. Overall, the module's mechanical structure and electrical joi nts remained stable following the −50 °C, 24 h freezing protocol. The absence of macroscopic damage (fracture, delaminati on, connector loosening, or leakage) supports the premise that subsequent changes in electrical performance can be analyze d largely independent of confounding mechanical degradation, thereby providing a clean basis for pre-/post-freezing compa risons.

3.2. Performance Analysis

To quantify performance changes induced by cryogenic storage, we compared the module's discharge capacity, direct-current internal resistance (DCIR), and insulation resistance before and after freezing. Tests followed the KC10031 framework, and evaluation metrics included module-level charge/discharge curves and DCIR evolution. Summary results are presented in Figure 5 and Figure 6.

3.2.1. Comparison of Discharge Capacity and DCIR Before vs. After Freezing

High-fidelity measurements of discharge capacity and DCIR were performed to assess electrical performance changes attributable to the −50 °C, 24 h freezing protocol. Figure 5a–b report the pre-freezing voltage/current traces and the corresponding DCIR profile; Figure 5c–d present the same measurements under identical protocols after freezing. In all graphs, red denotes voltage (V) and blue denotes current (A). Numerically, the pre-freezing discharge capacity was 158.90 Ah, with DCIR of 5.458 mΩ and insulation resistance ≥ 500 MΩ. After freezing, the discharge capacity measured 159.18 Ah (a +0.28 Ah change, ≈ +0.18%), while DCIR remained at 5.458 mΩ; insulation resistance likewise stayed ≥ 500 MΩ. These results indicate that the cryogenic pre-treatment did not degrade the module's electrical characteristics. The invariance of DCIR suggests that contact resistances (cell-tab/busbar interfaces, interconnects) and bulk ohmic contributions were unaffected. The stable insulation resistance implies no compromise of dielectric pathways or moisture-related leakage. The slight increase in measured capacity is within typical test repeatability and may reflect minor state-of-charge re-equilibration/balancing during the preconditioning sequence rather than a true improvement in active-material utilization. Overall, the freezing step preserved both rate-relevant resistance and usable capacity, supporting the feasibility of cryogenic storage/transport without detrimental impact on subsequent performance.

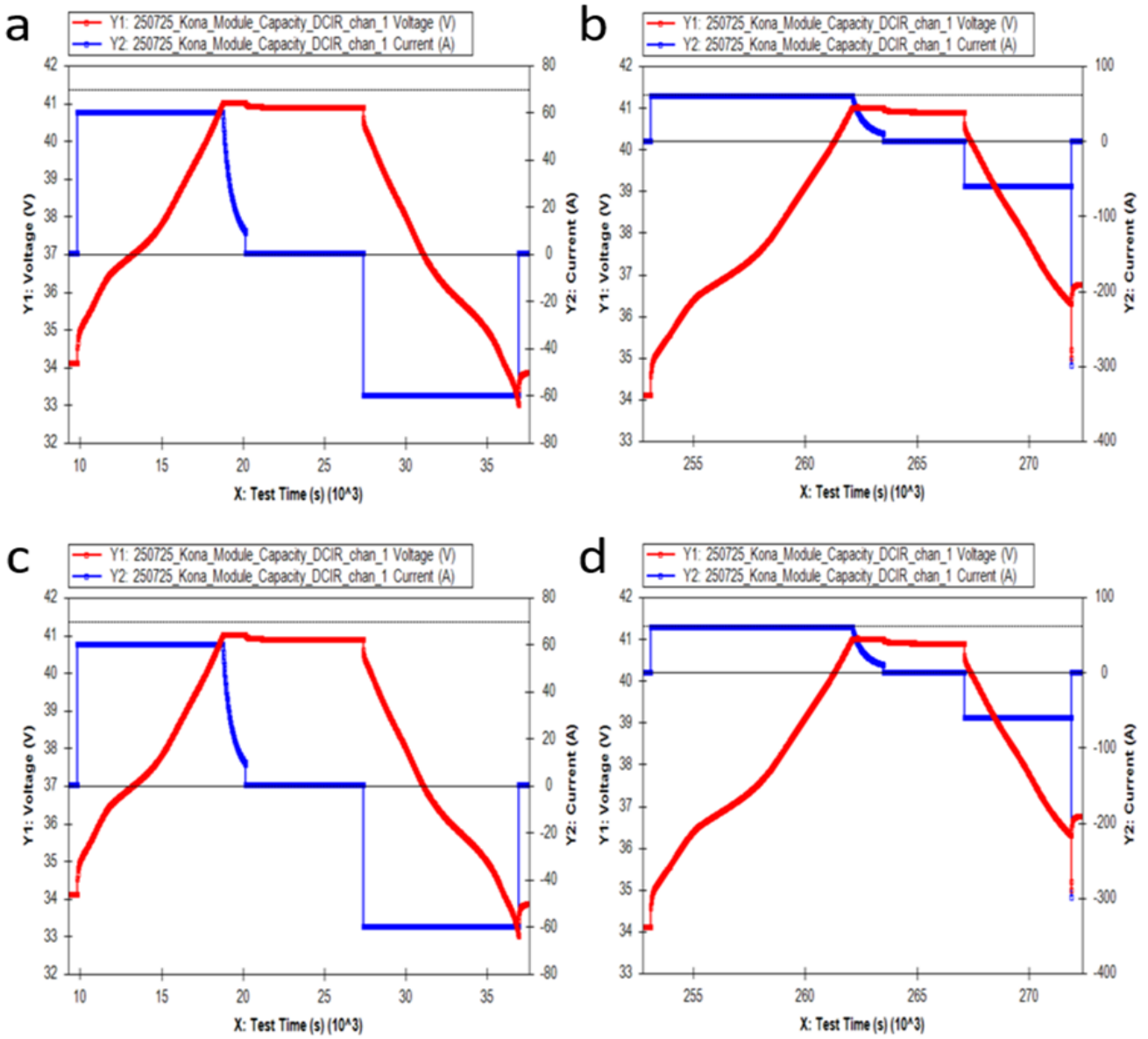

Figure 5.
Voltage and current profiles during charge/discharge cycle and DCIR tests of the used EV battery module before and after cryogenic freezing.
Note: (a) Voltage-current profile during charge/discharge before freezing; (b) DCIR measurement before freezing; (c) Voltage-current profile during charge/discharge after free zing; (d) DCIR measurement after freezing

3.2.2. Comparative Analysis of Electrical Performance Before and After Freezing

Figure 6 compares the module's charge/discharge curves and direct-current internal resistance (DCIR) before and after the freezing protocol. As shown in Figure 6a, the voltage–capacity profiles remain essentially unchanged pre- versus post-fr eezing: plateau regions and slope transitions are preserved, and no discernible distortion or polarization broadening is evide nt. In particular, the voltage trajectories during charge (~32–42 V) and discharge (~42–32 V) closely overlap for both condi tions, indicating that cryogenic storage did not measurably perturb the electrochemical reaction pathways or overpotential l andscape.

Quantitatively, the measured discharge capacity was 158.90 Ah before freezing and 159.18 Ah after freezing, correspo nding to a small absolute difference of +0.28 Ah (≈ +0.18%). Within typical test repeatability, this invariance supports the c onclusion that usable capacity is maintained following the −50 °C, 24 h exposure. The DCIR analysis (Figure 6b) likewise shows no change: both pre- and post-freezing values equal $5.458\times10^{-3}\Omega$ (5.458 mΩ), derived from the instantaneous voltag e response to programmed pulse-current steps (DCIR=ΔV/ΔI). The absence of any DCIR increase suggests that neither bul k ohmic pathways (tabs, busbars, interconnects) nor interfacial resistances (current collector/active-material, separator/elect rolyte) were degraded by the freezing/rewarming cycle. Together with the stable insulation resistance (≥ 500 MΩ), these fin dings indicate that dielectric integrity and electronic conduction paths remained intact. Overall, the overlapping voltage pro files, unchanged DCIR, and invariant capacity collectively demonstrate that the −50 °C storage protocol did not introduce measurable performance penalties at the module level. These results provide experimental support for the feasibility of low -temperature storage/transport of EOL EV battery modules without compromising subsequent charge–discharge behavior o r resistance characteristics, under the tested state-of-charge window and environmental conditions.

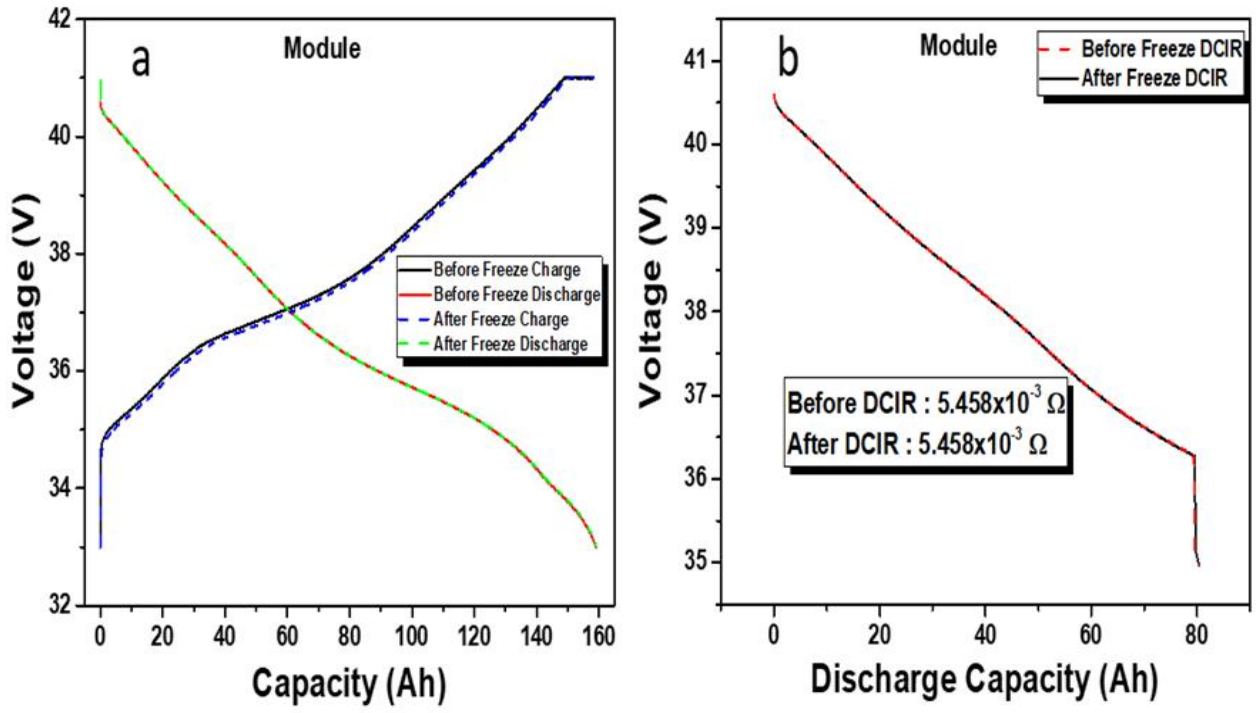

Figure 6.
Electrochemical performance of the battery module before and after cryogenic freezing.
Note: (a) Comparison of charge/discharge curves showing capacity retention before and after freezing treatment; (b) DC internal resistance (DCIR) measurement indicating neg ligible difference between pre- and post-freezing states (5.458×10^{-3} Ω in both cases).

4. Conclusions

This study quantitatively evaluated the effects of cryogenic storage on the electrical safety and performance of an end-of-life (EOL) EV battery module (3P10S, KONA EV). A controlled protocol (−50 °C, ≥24 h; electrically isolated; gradual rewarming) was applied, followed by like-for-like diagnostics.

1. Mechanical/visual integrity. Post-freezing inspection revealed no macroscopic deformation, swelling, leakage, delaminat ion, connector loosening, or corrosion in the cell array, busbars/connectors, or BMS assemblies. Adhesive interfaces exhibit ed localized stiffening but retained interfacial contact, suggesting negligible thermo-mechanical damage under the tested co ndition.
2. Electrical safety. Open-circuit voltage and insulation resistance (500 V DC, 60 s) showed no degradation after freezing (i nsulation ≥ 500 MΩ in both states), indicating preserved dielectric pathways and absence of moisture-induced leakage.
3. Electrochemical performance. Charge/discharge curves overlapped before and after freezing, with plateau regions and sl opes essentially unchanged. The measured discharge capacities were 158.90 Ah (pre) and 159.18 Ah (post), and DCIR rem ained constant at 5.458 mΩ. Together, these results indicate that the −50 °C storage did not measurably affect usable capaci ty or ohmic/interfacial resistance at the module level.
4. Implication for logistics. Within the tested window (−50 °C, 24 h, controlled ramp/soak), cryogenic storage is compatibl e with subsequent module operation and electrical safety, supporting its feasibility as a risk-mitigation measure for EOL bat tery handling, storage, and transport.
5. Limitations and future work. This assessment used a single module and a single temperature/soak condition; shock/penet ration abuse tests under cryogenic exposure, repeated freeze–thaw cycling, broader state-of-charge windows, and coolant al ternatives (e.g., LN_2 vs. liquefied air) should be examined. Long-term materials effects (adhesive embrittlement, gasket/seal integrity) and pack-level thermal gradients also warrant study.

References

[1] X. Feng, D. Ren, X. He, and M. Ouyang, "Mitigating thermal runaway of lithium-ion batteries," *Joule*, vol. 4, no. 4, pp. 743-770, 2020. https://doi.org/10.1016/j.joule.2020.02.010
[2] S. Shahid and M. Agelin-Chaab, "A review of thermal runaway prevention and mitigation strategies for lithium-ion batteries," *Energy Conversion and Management: X*, vol. 16, p. 100310, 2022. https://doi.org/10.1016/j.ecmx.2022.100310
[3] X. Xiao, B. Chen, X. Jin, Q. Zeng, Y. Tian, and Q. Li, "Experimental study on the effect of synergistic extinguishing method based on liquid nitrogen on lithium-ion battery fire after thermal runaway," *Fire*, vol. 7, no. 12, p. 479, 2024. https://doi.org/10.3390/fire7120479
[4] T. R. B. Grandjean, J. Groenewald, and J. Marco, "The experimental evaluation of lithium ion batteries after flash cryogenic freezing," *Journal of Energy Storage*, vol. 21, pp. 202-215, 2019. https://doi.org/10.1016/j.est.2018.11.027
[5] Sunderlin N. et al, "Thermal runaway behavior of cryogenically frozen lithium-ion cells under mechanical abuse," *Journal of Energy Storage* vol. 72, p. 108216, 2023.
[6] G. Zhang, Z. Li, H. Wang, and D. Yuan, "Study on the suppression effect of cryogenic cooling on thermal runaway of ternary lithium-ion batteries," *Fire*, vol. 5, no. 6, p. 182, 2022. https://doi.org/10.3390/fire5060182

[7] Z. Huang, P. Liu, Q. Duan, C. Zhao, and Q. Wang, "Experimental investigation on the cooling and suppression effects of liquid nitrogen on the thermal runaway of lithium ion battery," *Journal of Power Sources*, vol. 495, p. 229795, 2021. https://doi.org/10.1016/j.jpowsour.2021.229795

[8] Z. Huang *et al.*, "Preventing effect of liquid nitrogen on the thermal runaway propagation in 18650 lithium ion battery modules," *Process Safety and Environmental Protection*, vol. 168, pp. 42-53, 2022. https://doi.org/10.1016/j.psep.2022.09.044

[9] Z. Fang *et al.*, "Exploring the viability of cryogenic freezing for safe pretreatment in lithium-ion battery recycling," *Renewable Energy*, vol. 252, p. 123481, 2025. https://doi.org/10.1016/j.renene.2025.123481

[10] A. García, J. Monsalve-Serrano, R. L. Sari, and S. Martínez-Boggio, "Thermal runaway evaluation and thermal performance enhancement of a lithium-ion battery coupling cooling system and battery sub-models," *Applied Thermal Engineering*, vol. 202, p. 117884, 2022. https://doi.org/10.1016/j.applthermaleng.2021.117884